Journal of Alloys and Compounds 509 (2011) 1550–1553

Contents lists available at ScienceDirect

Journal of Alloys and Compounds

journal homepage: www.elsevier.com/locate/jallcom

In situ investigation of SnAgCu solder alloy microstructure

Alena Pietriková[a,*], Jozef Bednarčík[b], Juraj Ďurišin[a]

[a] Department of Technologies in Electronics, Faculty of Electrical Engineering and Informatics, Technical University of Ko˘sice, Ko˘sice, Slovak Republic
[b] Deutsches Elektronen-Synchrotron (DESY), HASYLAB, Notkestrasse 85, D-22603 Hamburg, Germany

ARTICLE INFO

Article history:
Received 11 June 2010
Received in revised form
23 September 2010
Accepted 26 September 2010
Available online 11 November 2010

Keywords:
SnAgCu solder alloy
Microstructure
In situ X-ray diffraction
Soldification process
β-Sn thermal expansion coefficient

ABSTRACT

In situ X-ray diffraction experiments, using synchrotron radiation, were employed to analyze microstructure evolution of the 96.5Sn3Ag0.5Cu (wt.%)—SAC305 lead-free solder alloy during heating (30–240 °C), isothermal dwell (240 °C) and cooling (240–30 °C). The special emphasis was placed on the study of the melting and solidification processes, explaining formation, distribution and the order of crystallization of the crystal phases (β-Sn, intermetallic compounds) in the solder alloy. Furthermore, thermal expansion behaviour of the main constituent phase β-Sn was analyzed prior to melting and after the consequent solidification.

1. Introduction

Lead-free solders based on SnAgCu alloys (with melting temperature usually under 220 °C) are extensively used as solder materials in the electronic industry. Numerous studies have revealed that additions of transition metals in SnAgCu alloys normally result in important microstructure modification and improvement of mechanical properties [1]. Microstructure of solder joints of final electronic devices are generally defined by the applied solder alloy, the process of soldering, the composition of soldered materials and the utility of the final device. All four factors have significant impact on phase transformations in solder joints consequently influencing their properties. The formation of solder joints are based on the melting of the solder alloy, the reaction of the alloy with the soldered surface and the solidification of the solder alloy. The microstructure of the most widespread SAC305 off-eutectic alloy consists of large β-Sn dendritic crystals with typical size of 10^1–10^2 μm. Crystal phases such as β-Sn and fine Ag_3Sn precipitates (≈1–10^1 μm) are excluded from eutectics. Ag_3Sn precipitates are preferentially distributed within interdendritic regions whereas Cu_6Sn_5 intermetallic compounds (≈1 μm) are distributed in the volume of the dendrites [2].

Our study realized by in situ measurements gives an apt real-time record of behaviour of the SAC305 alloy during temperature increase (30–240 °C), dwell (240 °C) and temperature decrease (240–30 °C), thus simulating the reflow soldering process. The special emphasis is placed at the observation of the phase evolution and thermal expansion of the main constituent β-Sn phase.

2. Experimental details

The temperature evolution of the microstructure of the SAC305 (solidus/liquidus 217/220 °C [3]) solder alloy was investigated by in situ angular dispersive X-ray diffraction (XRD) using the powder diffractometer at the B2 bending magnet beamline of the DORIS III positron storage ring in HASYLAB/DESY (Hamburg, Germany). The beamline allows the performance of X-ray diffraction measurements in Debye–Scherrer geometry (Fig. 1). In situ experiments were performed using a STOE furnace. More details about the B2 beamline design and parameters can be found in [4]. For our measurements the wavelength was set to $\lambda = 0.537545$ Å (equivalent to the photon energy 23.06 keV). The use of synchrotron radiation has numerous advantages in comparison with conventional laboratory X-ray lamps since it offers high brilliance photon beams, covering a relatively wide energy spectrum. High-energy high-flux photon beams, available at the B2 beamline, are perfectly suited for in situ investigation of lead-free solder alloys in transmission geometry. To speed up the measuring, diffracted X-rays were detected on a position-sensitive image plate detector OBI, covering the angle range $2\theta_{max} = 110°$.

The sample of the alloy in the form of flaky swarf was put (in open air) into a glass capillary having the inner diameter of 0.28 mm. The capillary containing the sample was mounted in to the STOE furnace. The heating was realized by a resistive graphite element. The temperature in the sample vicinity was measured by a thermocouple. To eliminate the texture effect and to ensure correct intensities of the Bragg peaks, the capillary was rotating with a frequency of 2 Hz around its horizontal axis, perpendicular to the incoming monochromatic beam (Fig. 1). The sample was illuminated with the monochromatic beam having the width and height of 12 and 5 mm, respectively. Since the intensity of the incoming beam decays due to time decay of the positron current in the storage ring, exposure was defined by achieving the preset number of photons detected by an incoming beam monitor. Such a procedure yields data normalized to the incoming beam intensity and thus simplifies further analysis. Measurement at every temperature took from 12 to 14 min. A

* Corresponding author. Tel.: +421 55 602 3194; fax: +421 55 602 3195.
E-mail address: alena.pietrikova@tuke.sk (A. Pietriková).

0925-8388/$ – see front matter © 2010 Elsevier B.V. All rights reserved.
doi:10.1016/j.jallcom.2010.09.153

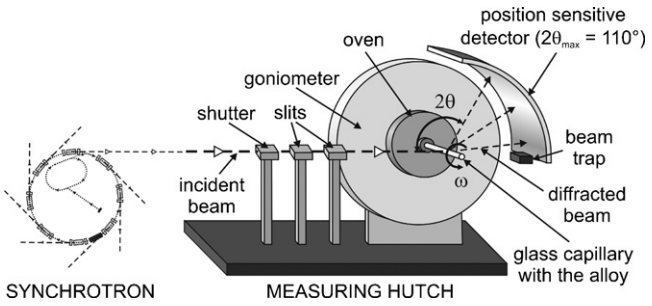

Fig. 1. Configuration of the diffractometer in Debye–Scherrer geometry.

temperature step of 10 °C was used during th heating and cooling, whereas the 2 °C step was applied for more detailed inspection of the melting and the solidification processes occurring at the temperature ranges of (220–240 °C) and (240–190 °C), respectively.

3. Results and discussion

3.1. The melting and solidification process

The X-ray diffraction pattern of the fresh sample taken at 30 °C reveals the presence of the sharp and intense Bragg peaks stemming from the β-Sn phase (PDF Nr. 4-673), which can be found in crystallographic database [5]. Furthermore, slight traces of Ag_3Sn (PDF Nr. 44-1300) crystal phase are clearly visible (Fig. 2a). This measurement is further used as a reference for all other XRD measurements. From the comparison of details of the diffraction patterns acquired at 30 °C in the initial state (Fig. 2a) and in the final state (after the melting and solidification—Fig. 2b), it is clear, that after the re-melting, two new phases were formed: Cu_6Sn_5 (PDF Nr. 45-1488) and as a product of β-Sn oxidation also SnO (PDF Nr. 6-395). The heating and cooling of the in situ XRD experiment is further discussed in the following paragraph.

Heating the sample from 30 up to 224 °C reveals practically no phase changes, except the appearance of slight traces of SnO (Fig. 3). The most probable explanation is the surface oxidation of the solder flakes due to the presence of residual oxygen entrapped between particles while sealing the capillary in open air. After reaching a temperature of 224 °C diffraction peaks, belonging to major constituent phase β-Sn, rapidly diminish, which is a sign of reaching the melting point of the SAC305 solder (Fig. 3). The XRD pattern acquired at 228 °C reveals weak traces of the β-Sn phase together with a diffused background due to the X-rays scattering from the amorphous glass capillary. The X-ray diffraction pattern obtained at 230 °C exhibits no Bragg peaks at all and thus completely confirms a molten state of the SAC305 alloy. It should be noted here

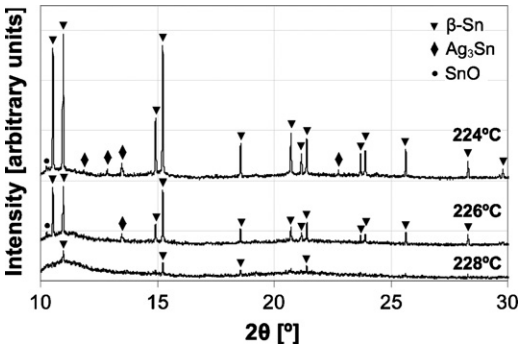

Fig. 3. Comparison of the diffraction patterns of the SAC305 alloy at selected temperatures during heating.

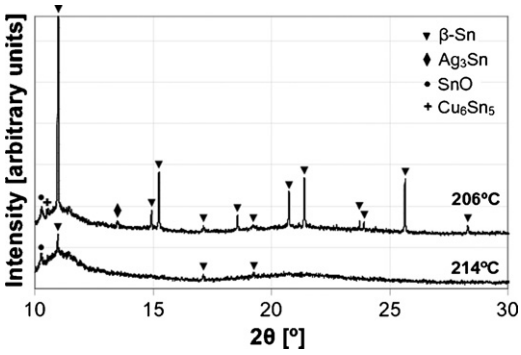

Fig. 4. Comparison of the diffraction patterns of the SAC305 alloy at selected temperatures during cooling.

that according to values published in the database [3], the liquidus temperature of SAC305 is 220 °C, i.e. by 10 °C lower than obtained value. Such discrepancy could originate from the temperature gradient inside the furnace. Further isothermal dwell at 240 °C for 2 h reveals no changes and the diffuse character of the XRD patterns remained unaffected.

In the next part we focused on the solidification behaviour of the SAC305 solder when cooled from 240 down to 30 °C. XRD patterns revealed a diffuse character specific for amorphous materials up to a temperature of 214 °C, when the first Bragg peaks corresponding to the major β-Sn phase appear (Fig. 4). A similar diffraction pattern (if only β-Sn reflections are taken into consideration) was recorded during a temperature increase (melting process) in the temperature interval of 226–228 °C (Fig. 3). One may conclude here that the temperature difference of 12–14 °C, between the melting and the solidification, indicates a kind of thermal hysteresis. Further low-

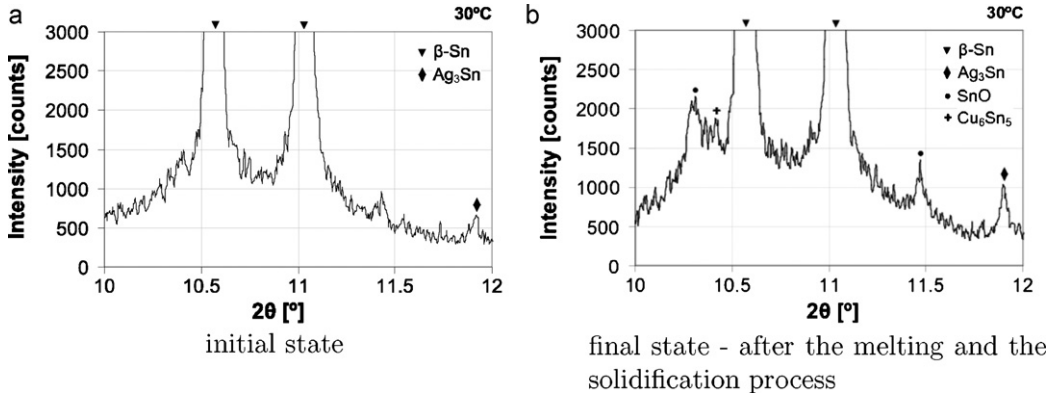

Fig. 2. Detail of the diffraction pattern of the SAC305 alloy at 30 °C.

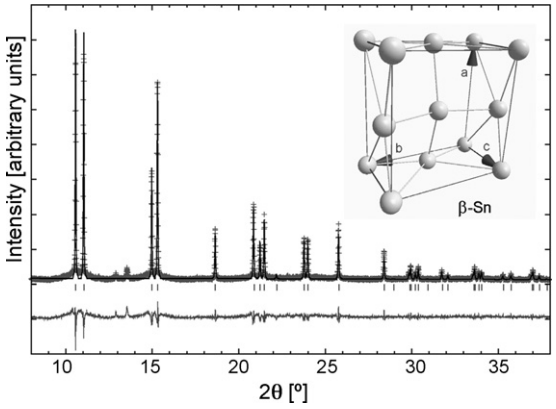

Fig. 5. The XRD pattern of the SAC305 alloy at 30 °C. Observed and fitted intensities are plotted with crosses and full line, respectively. The difference curve and positions of Bragg peaks are also depicted. The inset shows the unit cell of the tetragonal β-Sn phase.

ering of the temperature, down to 206 °C, leads to the formation of a minor Ag_3Sn phase (Fig. 4). The process of the crystallization ends approximately between 170 and 160 °C.

All this results are in good agreement with previous microscopic observations, showing that Cu_6Sn_5 is located almost exclusively in the volume of the β-Sn crystals, while Ag_3Sn is located only in interdendritic regions of β-Sn—solidification proceeds with the formation of the β-Sn and Cu_6Sn_5 phases followed by the crystallization of Ag_3Sn [6].

3.2. The determination of the thermal expansion coefficient

The thermal expansion coefficient is the most important parameter describing thermally induced stresses in the volume of the solder alloy in solder joints. Thermally induced stresses manifest themselves at various levels, from the joints' area to package-level and to interconnection-level of the electronic components. Nowadays many problems occur at the interconnection level, for example, the failure of solder joints forms a large proportion of the total number of fatigue failures in surface-mounted electronic devices. This represents a serious issue in the area of mounting technologies in electronics. Therefore the knowledge of the thermal expansion behaviour is of great importance.

As concluded from previous observations, β-Sn tetragonal phase (space group 141, $a = b = 5.819$ Å, $c = 3.1753$ Å, $\alpha = \beta = \gamma = 90°$, see the inset in Fig. 5) is the main constituent phase of the SAC305 solder. The quantitative microstructure (unit cell parameters) analysis of investigated material was performed using the full-pattern fitting Rietveld method implemented in a software package GSAS [7]. As can be seen from Fig. 5 a reasonable match, between the observed and fitted intensities, was achieved. Furthermore, we were interested in how the unit cell parameters, of the β-Sn, evolve during thermal cycling, during the heating from room temperature to above the melting point and consequently cooling back down to room temperature. The series of XRD patterns, acquired during heating and cooling, were, in successive steps, quantitatively analyzed using the GSAS program.

The Rietveld refinement procedure of the β-Sn phase for an individual XRD pattern, acquired at a temperature T, yields a set of Bragg reflections characterized with the Miller indices $(h\,k\,l)$ and corresponding $2\theta_{hkl}$ values. According to the Bragg law we can write for each reflection the following equation

$$2d_{hkl} = \lambda / \sin\theta_{hkl}, \tag{1}$$

in which d_{hkl} denotes the interplanar distance, λ is the wavelength and θ_{hkl} is the Bragg angle of the first order reflection. In the case of a tetragonal crystal system, the relation between interplanar distance d_{hkl}, Miller indices h, k, l and unit cell parameters a and c can be written in the form [8]

$$1/d_{hkl}^2 = \left(h^2 + k^2\right)/a^2 + l^2/c^2. \tag{2}$$

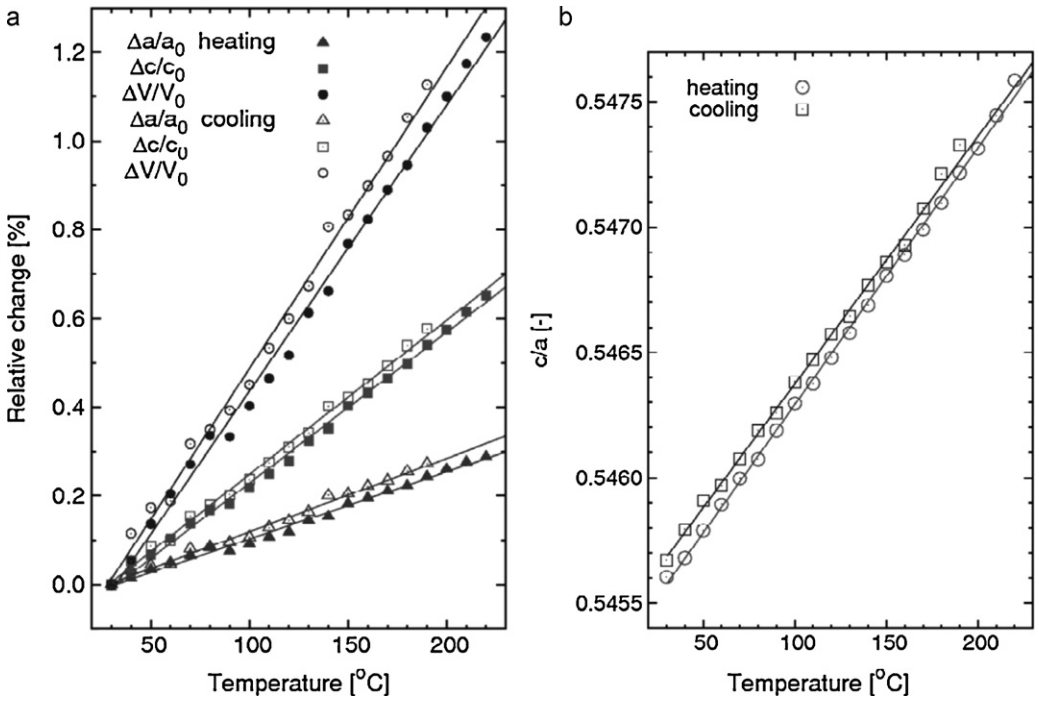

Fig. 6. (a) The relative change of the unit cell parameters a, c and V with temperature. Filled and open symbols correspond to the heating and cooling, respectively. (b) Temperature behaviour of c/a ratio for the tetragonal β-Sn phase. The size of points refers to the experimental uncertainties. The full lines represented fit the data.

Table 1
Comparison of calculated β_a, β_c and α_V of the β-Sn tetragonal unit cell.

[$\times 10^{-5}$ K^{-1}]	Heating (30–240 °C)	Cooling (240–30 °C)
β_a	1.52 ± 0.03	1.66 ± 0.05
β_c	3.40 ± 0.04	3.48 ± 0.05
α_V	6.44 ± 0.11	6.79 ± 0.14

Combining Eqs. (1) and (2), one obtains the following equation

$$\left(\frac{h^2+k^2}{a^2}\right)+\frac{l^2}{c^2}=\frac{4}{\lambda^2}\sin^2\theta_{hkl}, \quad (3)$$

which can be written for every Bragg reflection of the tetragonal β-Sn phase. This results in an overdetermined system of linear equations with respect to $1/a^2$ and $1/c^2$, which can be solved by the linear least squares method [9].

Fig. 6a shows relative changes of the unit cell parameters a, c and V (unit cell volume) with respect to the reference values a_0, c_0 and V_0 determined at the reference temperature $T_0 = 30$ °C. All unit cell parameters reveal a linear temperature dependence. Furthermore, one can also conclude that the heating curves show slightly lower slopes than the corresponding cooling curves. We fit the data to the following equations

$$\frac{\Delta a}{a_0}=\beta_a(T-T_0), \quad (4)$$

$$\frac{\Delta c}{c_0}=\beta_c(T-T_0), \quad (5)$$

$$\frac{\Delta V}{V_0}=\alpha_V(T-T_0) \quad (6)$$

corresponding to the linear and volume thermal expansion coefficients, β_a, β_c and α_V, respectively. Heating and cooling parts were fitted separately. The obtained linear and volume thermal expansion coefficients, β_a, β_c and α_V, respectively, are summarized in Table 1. As can be seen in Fig. 6b, the temperature dependence of the c/a ratio of the tetragonal β-Sn phase shows linear dependence on temperature. However, the heating curve shows a slightly higher value of the slope as compared with the cooling curve. Extrapolating both fitted curves indicates that they would intersect at the temperature of 324 °C, which is far above the melting point (230 °C). It is also interesting to note that despite the fact that the c parameter is substantially smaller than parameter a, it exhibits a significantly higher linear expansion coefficient.

4. Conclusions

In situ X-ray diffraction experiments enabled detailed analysis of the melting and solidification process of the SAC305 alloy. It was found that the SAC305 solder melts at 230 °C. When cooling from 240 °C the SAC305 alloy solidifies at the temperature of 214 °C. During solidification, β-Sn and Cu_6Sn_5 is also formed. Formation of Ag_3Sn occurs at 206 °C and the remaining amount of alloy crystallizes approximately at 160 °C. Furthermore, observation of the thermal expansion behaviour of the β-Sn tetragonal unit cell revealed linear dependence of the unit cell volume on temperature. The unit cell parameters a and c also increase linearly with the temperature. Despite the fact that the c parameter is substantially smaller than parameter a, it exhibits a significantly higher linear thermal expansion coefficient. Comparison between data obtained during heating and cooling indicates that the thermal expansion coefficient is slightly greater in the case of cooling.

Acknowledgments

The authors wish to thank Dr. H. Franz and Dr. D. Trots from HASYLAB/DESY (Hamburg, Germany) for their help with the experiments. J.D. acknowledges the financial support from HASYLAB/DESY allowing his participation at the experiments.

References

[1] I.E. Anderson, Journal of Material Science: Materials in Electronics (2006).
[2] B.A. Cook, I.E. Anderson, J.L. Harringa, S.K. Kang, Journal of Electronic Materials 32 (12) (2003).
[3] Cooperation on Science and Technology, European Lead-free Soldering Network: Database for Properties of Lead-free Solder Alloys, February 2006.
[4] M. Knapp, C. Bähtz, H. Ehrenberg, H. Fuess, Journal of Synchrotron Radiation 11 (2004) 328–334.
[5] The International Centre for Diffraction Data®: PDF-2, 1997.
[6] A. Pietriková, J. Ďurišin, J. Urbančík, J. Banský, in: ISSE 2009: 32nd International Spring Seminar on Electronics Technology: Hetero System Integration, the Path to New Solutions in the Modern Electronics, 2009, pp. 1–5, ISBN 978-1-4244-4260-7.
[7] A.C. Larson, R.B. Von Dreele, General Structure Analysis System (GSAS), Los Alamos National Laboratory Report LAUR 86-748, 2004.
[8] V.K. Pecharsky, P.Y. Zavalij, Fundamentals of Powder Diffraction and Structural Characterization of Materials, KLUWER Academic Publishers, 2003, ISBN 1-4020-7365-8.
[9] S.J. Miller, The Method of Least Squares, Brown University, Providence, 2006.